Analog Integrated Circuits and Signal Processing, 23, 227–236, 2000

An Improved Silicon Neuron

C. RASCHE AND R. DOUGLAS

*Institut für Neuroinformatik (ETHZ/UNIZ), Winterthurerstr 190, CH-8057 Zürich, Switzerland**

Received January 18, 2000; Accepted January 27, 2000

Abstract. We describe an improved spiking silicon neuron (SN) [6] that approximates the dynamics of ionic currents of a real nerve cell. The improved version has less circuitry and fewer parameters than previous circuits thereby improving the spiking characteristics. We describe the differential equations governing the revised circuits and use them to explain the spiking properties of the SN. We also describe how to tune the parameters efficiently to bring the neuron quickly into its correct operating regime. The new neurons are sufficiently robust for operation in large networks. We demonstrate their robustness by comparing the neuron's frequency-current curve between different chips for the same set of parameter values.

Key Words: neuromorphic system, conductance-based neuron model, spike frequency adaptation

1. Introduction

Previous SNs [6,10] suffered from oversensitivity to parameters. It was difficult to find a parameter space which elicits the desired spiking properties. The reason for the instability laid in the many parameters and unbalanced circuit parts. The circuits required two major improvements. First, the parameter values should be easy to find. Second, these parameter values should be sufficiently stable, to be stored on-chip by floating-gate technology.

Fig. 1 is a simplified electrical diagram of the silicon neuron circuitry. The left diagram summarizes the somatic ionic conductances of our neuron model in a parallel conductance model [5]. The right diagram shows a model of the intracellular calcium concentration. The separation into a soma equivalent and a calcium model is based on location of these processes. Another kind of separation we make is based on function: The basic spike mechanism, and the adaptation mechanism. The basic spike mechanism represents the spiking behavior of the neuron and contains both a passive component and a spike component. The passive component simulates the passive behavior of the neuron. The spike component contains the actual mechanism that generates spikes [4]. The adaptation mechanism is responsible for spike-frequency adaptation and bursting and relies on the after-hyperpolarization (AHP) conductance and the calcium model [5].

The soma equivalent can be expressed in terms of currents as follows:

$$I_{Cm} = I_{Leak} + I_{Na} + I_{Kd} + I_{AHP} + I_{Inj} \qquad (1)$$

where I_{Cm} is the current across the membrane capacitance, I_{Inj} is the stimulation current (either synaptic or injected input, not shown in Fig. 1), I_{Leak} is the leakage current, I_{Na} is the sodium current, I_{Kd} is the potassium current and I_{AHP} is the after-hyperpolarization current. The arrows across the spike conductances indicate that these conductances have an explicit voltage and time dependence.

The calcium model is a model of the intracellular calcium concentration, V_c. Every time a spike occurs, V_c increases through influx of calcium ions (I_{Cain}) into the soma [13]. In Fig. 1 this trigger of calcium influx is indicated by the grey arrow (labelled ''spike discriminator''), pointing from the membrane potential, V_m, to the switch in the calcium model. The calcium concentration decays (I_{Cabuf}) towards a resting concentration due to intracellular processes like, e.g. buffering [5]. The calcium model can be expressed in terms of currents as follows:

$$I_{Cc} = I_{Cain} + I_{Cabuf} \qquad (2)$$

*Please address correspondence to rasche@klab.caltech.edu or C. Rasche, Caltech, Division of Biology 139-74, Pasadena, CA 91125, USA

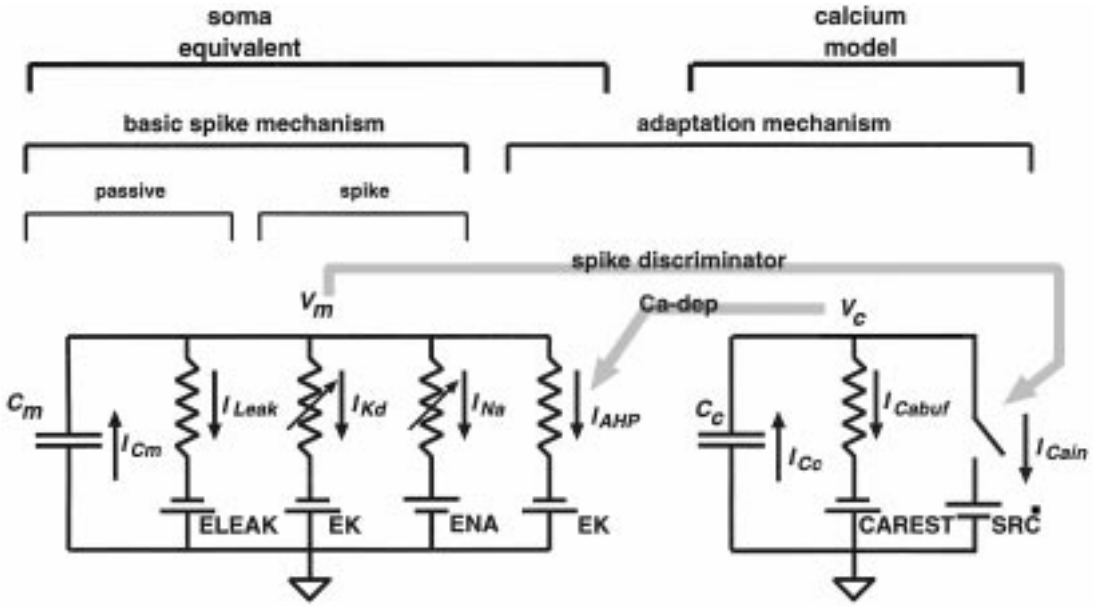

Fig. 1. Electrical diagram of the neuron circuitry. Left part ''soma equivalent'': Parallel conductance model for ionic currents in a membrane. V_m, membrane potential; C_m, membrane capacitance; ELEAK, resting potential; EK, potassium reversal potential; ENA, sodium reversal potential. Right part ''calcium model'': A model for the intracellular calcium concentration. C_c, calcium concentration (voltage); C_c, calcium buffer (capacitance); CAREST, calcium resting concentration; SRC, calcium source. See text for further explanations.

where I_{Cc} is the current across the calcium capacitance. When the spike frequency of the neuron increases the calcium concentration rises. A higher calcium concentration increases the AHP current, which in turn inhibits V_m, leading to spike-frequency adaptation. In Fig. 1, this negative feedback loop is indicated by the grey arrow (labelled ''Ca-dep''), pointing from V_c to the AHP current.

2. Methods

The building blocks used in our SN circuits are the transconductance amplifier (TCA), the follower integrator (FI), the current mirror (CM) and the half-wave rectifier [7]. We use the term ion conductance, e.g. sodium conductance, if we speak of the entire ion conductance circuit. We use the term ion current for the actual output of the ion conductance circuit. Fixed voltage parameters are noted by capitalized letters (e.g. ELEAK), state variables are noted by V (e.g. V_m).

2.1. The Basic Spike Mechanism

The basic spike mechanism is expressed by equation (1), neglecting the AHP current. We approximate the passive behavior of a neuron, a RC circuit, with a FI circuit (Fig. 2(a), left grey block, FI1). The input is a fixed voltage, ELEAK, representing the resting potential of the neuron. The output voltage, V_m, represents the membrane potential. The dependence of the leakage current, I_{leak}, on the membrane voltage, V_m, is given by current-voltage relationship of the TCA:

$$I_{Leak}(V_m) = I_{GLEAK} \tanh\big(c_T(ELEAK - V_m)\big) \qquad (3)$$

where I_{GLEAK} is the maximal bias current of the TCA. The parameter c_T, combines the constants which are associated with a TCA [7].

The sodium current, I_{Na}, is generated by subtraction of an activation current, I_m, and an inactivation current, I_h (Fig. 2(a), upper middle grey block). The activation current rapidly turns on by a fast positive feedback loop implemented by TCA1 and CM2. The

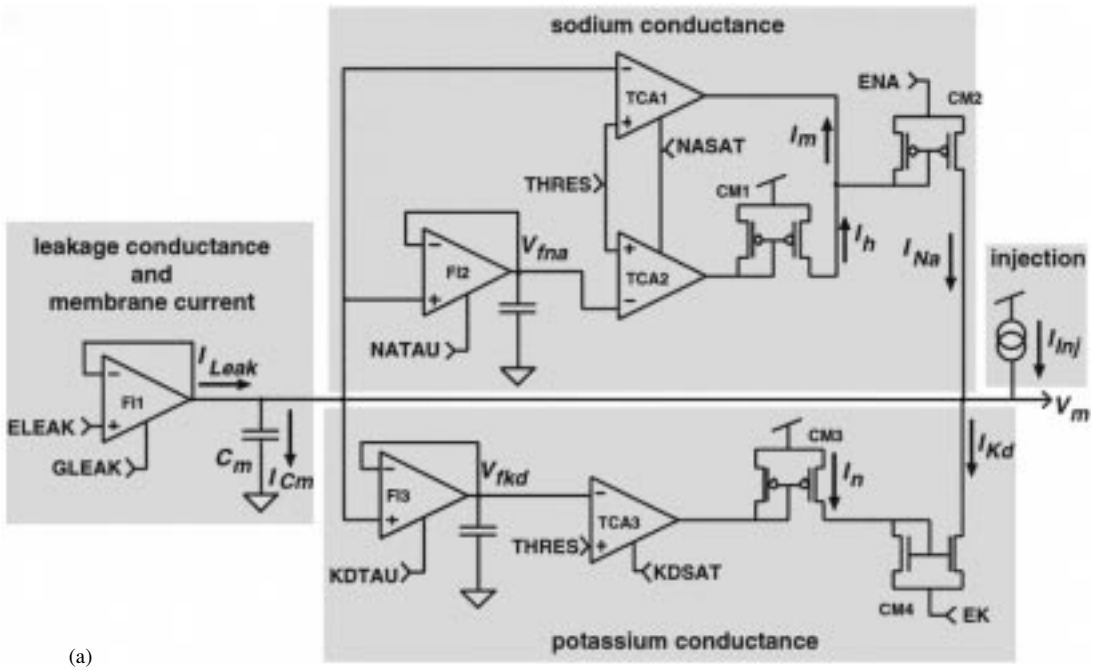

(a)

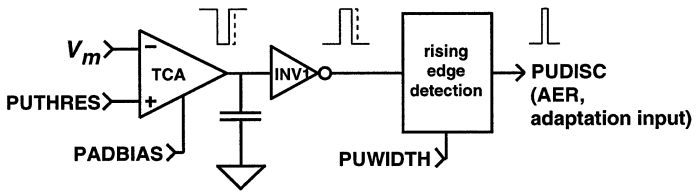

(b)

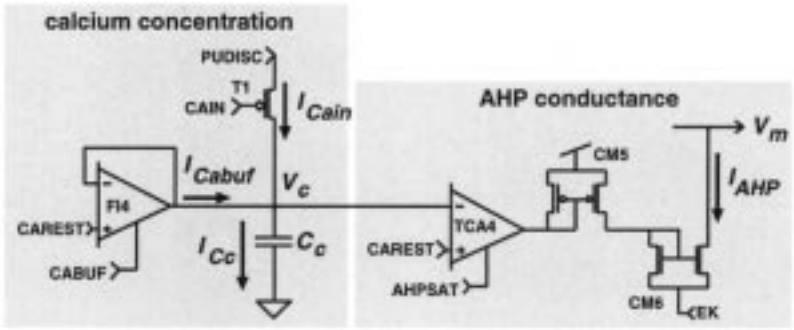

(c)

Fig. 2. Neuron circuitry. (a) The basic spike mechanism: The horizontal wire represents the membrane potential, V_m. The grey boxes mark the various ion current circuits and the injection current. (b) Spike discriminator. (c) Adaptation mechanism. The left grey box contains circuitry to simulate the calcium concentration. The right grey box contains circuitry for generation of the after-hyperpolarization (AHP) current. See the method section for a detailed description.

inactivation current turns on by a slower negative feedback loop, implemented by FI2, TCA2, CM1 and CM2. Because the positive feedback loop constitutes a half-wave rectifier, we can summarize the sodium current as follows:

$$I_{Na}(V_m, t) = \big(I_m - I_h(t)\big)\theta(V_m - THRES) \tag{4}$$

where θ is the Heaviside function: $\theta(x) = 0$ for $x \leq 0$ and $\theta(x) = 1$ for $x > 0$. As long as V_m is below the spiking threshold, THRES, I_{Na} is zero. When V_m rises above THRES, the activation current I_m rapidly turns on by the positive feedback loop, therefore we can set I_m to the maximal current of TCA1:

$$I_m = I_{NASAT} \tag{5}$$

The circuits that provide the inactivation of the sodium conductance contain another half-wave rectifier (TCA2 and CM1). Consequently, I_h is only generated if V_{fna} is above THRES. After the activation current has turned on, the follower voltage V_{fna} will rise above THRES due to the steeply rising V_m. Because FI2 operates then in the large signal domain, the output voltage ΔV_{fna} $(V_{fna} - \text{THRES})$ increases linearly with time:

$$\Delta V_{fna}(t) = \frac{I_{NATAU}}{C_f}(t - t_0) \tag{6}$$

where t_0 corresponds to the time, at which V_m crosses THRES (spike onset). I_{NATAU} is the maximal bias current of FI2, C_f is the follower capacitance. The inactivation current is then:

$$I_h(t) = I_{NASAT} \tanh\big(c_T \Delta V_{fna}(t)\big) \tag{7}$$

The sodium current can now be expressed by replacing the currents I_m and I_h in equation (4) by the expressions in equations (5) and (7):

$$I_{Na}(V_m, t) = I_{NASAT}\big(1 - \tanh\big(c_T \Delta V_{fna}(t)\big)\big) \cdot \theta(V_m - THRES) \tag{8}$$

Once the sodium current is fully turned on, it decays due to the tanh behavior.

The potassium conductance is only an activating conductance; it lacks an inactivation. It constitutes the second negative feedback loop implemented by FI3, TCA3, CM3 and CM4 (Fig. 2(a), lower middle grey block). The potassium conductance is on as long as the voltage V_{fkd} is above THRES, otherwise it is zero due to half-wave rectification:

$$I_{Kd}(V_m, t) = I_n \theta\big(\Delta V_{fkd}(t, V_m)\big) \tag{9}$$

The output voltage V_{fkd} increases linearly with time—in response to the quickly rising V_m—as it is the case for V_{fna}. ΔV_{fkd} $(V_{fkd} - \text{THRES})$ rises linearly as long as V_m is above V_{fkd}, and falls linearly when V_m is below V_{fkd}:

$$\Delta V_{fkd}(t, V_m) = \frac{I_{KDTAU}}{C_f}(t - t_0)) \cdot sign(V_m - \Delta V_{fkd}) + \Delta V_{fkd,t_1} \tag{10}$$

I_{KDTAU} is the maximal bias current of FI3. V_{fkd,t_1} is the initial condition when V_{fkd} starts to follow the decreasing V_m at time t_1. The current I_n can then be described as

$$I_n(t, V_m) = I_{KDSAT} \tanh\big(c_T \Delta V_{fkd}(t, V_m)\big) \tag{11}$$

I_{KDSAT} is the maximal bias current of TCA3. We rewrite equation (9) by replacing I_n by the expression given in equation (11):

$$I_{Kd}(V_m, t) = -I_{KDSAT} \tanh\big(c_T \Delta V_{fkd}(t, V_m)\big) \cdot \theta\big(\Delta V_{fkd}(t, V_m)\big) \tag{12}$$

I_{Kd} turns on and off with the same tanh-like dynamics. There is a minus sign in equation (12), because the potassium current is a negative current through CM4.

The positive feedback loop of the sodium conductance could be suppressed by an early onset of the two negative feedback loops due to device mismatch. To guarantee that the negative feedback loops turn on later, FI2 and FI3 are sealed in such a way that the voltage output lags with respect to V_m by a few millivolts. We did that by using a wide diode-connected transistor (12 μm instead of 6 μm) in the current mirror of the TCA. We also have to ensure that the sodium inactivation completely turns off the activation, by using a wider bias transistor (12 μm) for TCA2 than for TCA1.

2.2. *Spike Discriminator*

The purpose of the spike discriminator is to generate a pulse of fixed width, PUDISC, in response to a membrane spike (Fig. 2(b)). PUDISC is used as input to the adaptation mechanism as well as for the address-event representation (AER) system connecting neurons [1].

The parameter PUTHRES determines the

threshold of pulse generation. The parameter PADBIAS is the chip's bias parameter. As long as V_m is below PUTHRES, the voltage output of the TCA is high otherwise (during a membrane spike) it is low. The subsequent inverter, INV1, generates a proper pulse, which still pulse depends on the actual membrane spike width. As the membrane spike width may vary for different stimulation currents and can make tuning difficult, we added an edge-detection circuit that generates pulses of fixed width. The edge-detection circuit is standard digital circuitry and contains a RS-flip-flop [2]. The parameter PUWIDTH is a bias voltage and sets the desired pulse width of PUDISC.

2.3. Adaptation Mechanism

The input to the adaptation circuit is the pulse PUDISC applied to the source of transistor T1. CAIN determines the calcium influx (represented by I_{Cain}) into the neuron that occurs during each spike. The voltage, V_c, on the capacitance C_c, represents the intra-cellular calcium concentration. V_c decays towards a resting concentration by I_{Cabuf}, which is the output of a follower-connected wide-range-input TCA (FI4) [14]. CAREST sets the voltage for the calcium resting concentration. The current I_{Cabuf} is analogous to the leakage current (equation (3)).

The AHP conductance circuitry is analogous to the potassium conductance circuitry TCA3, CM3 and CM4 and is simply expressed by the equation of the TCA. The calcium current is integrated onto the V_m node, thereby forming a slow negative feedback loop causing the spike-frequency adaptation.

The transistors of FI4 are sealed in the same way as FI2 and FI3. This guarantees that the AHP current does not strongly leak, due to device mismatch, when the neuron is at rest. Otherwise, tuning of the adaptation characteristics can be difficult.

3. Results

A chip of approximately $2 \times 2\,\mathrm{mm}^2$ was fabricated using a standard $1.2\,\mu$m CMOS technology. Transistors sizes are generally $6\,\mu$m by $6\,\mu$m. We chose such a large size, because our $1.2\,\mu$m process choice is less well controlled compared to our previous choice, a $2.0\,\mu$m process. In the digital circuitry (spike discriminator), transistors are miminum size. For some of the bias transistors we chose larger widths ($8\,\mu$m). The overall size of the layout is $662\,\mu\mathrm{m} \times 52\,\mu\mathrm{m}$.

The basic spike mechanism comprises 38 transistors (3 FI, 3 TCA, 4 CM) and 3 capacitances. The FI capacitances, FI2 and FI3, are about 0.4 nF each. The adaptation circuit comprises 20 transistors and 1 capacitance. The capacitance C_c we estimate 0.6 nF. The spike discriminator has 20 transistors. C_m is about 7 nF. Current injection to the neuron is mediated by a p-type transistor. We report the amount of injection either as a gate voltage or as an approximate current.

To tune the passive behavior of the neuron we stimulate it with step currents. When the step current is turned off, the slope of the falling V_m is solely determined by the leakage current. To obtain optimal spiking properties, we tune GLEAK such that the slope (in the large signal domain) is tuned to a value of about 500 mV/15 ms.

Fig. 3 shows the shape of a single spike extracted of a spike train (as for example in Fig. 4). Before the membrane spike the follower voltages V_{fkd} and V_{fna} follow V_m smoothly with a DC-offset of about -100 mV due to the sealed followers. During, and

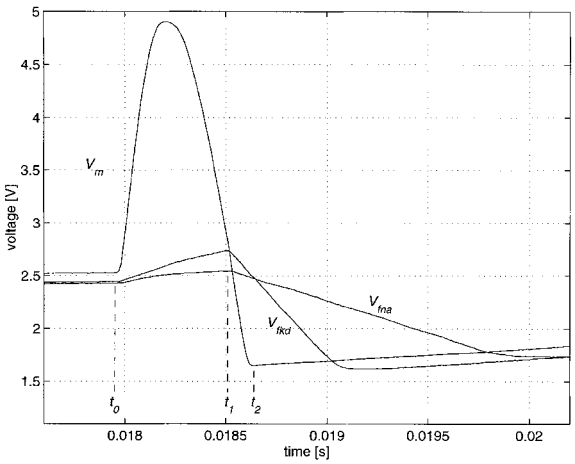

Fig. 3. Trace of a single V_m spike and the follower voltages V_{fna} and V_{fkd}. t_0 is spike onset, t_1 is the time where V_{fkd} starts to decay, t_2 is spike offset. ELEAK = 2.0 V, GLEAK = 0.38 V, THRES = 2.50V, NATAU = 0.37 V, NASAT = 0.63 V, KDTAU = 0.43 V, KDSAT = 0.58 V, ENA = 5.0 V, EK = 1.5 V. Spike duration: 0.0179 s to 0.0186 s. Spike amplitude = 2.5 V (ENA-THRES).

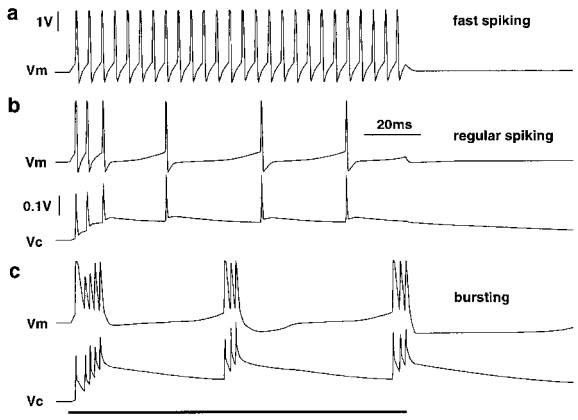

Fig. 4. Spiking characteristics. Response of the neuron to a step current of 120 ms (see black bar below). a. Fast spiking. Only the basic spike mechanism is turned on. Parameter values as in Fig. 3 (b). Regular spiking (with corresponding calcium level). Spike frequency adaptation caused by the AHP current. AHPSAT = 0.50 V. The peaks on V_c are caused by crosstalk from V_m. CABUF = 0.22 V, CAIN = 4.40 V, CAREST = 2.0 V. Current injection $\simeq$ 180 nA. (c) Bursting. AHP = 0.48 V, KDSAT = 0.41 V. The width of the initial spike in the first burst is larger than the remaining ones due to the weaker potassium current.

some time after the spike, the follower voltages rise and fall linearly, as predicted by equations (6) and (10). About 1 ms after spike offset, the follower voltages catch up with V_m again. The slope of the rising flank is shallower than the one of the falling flank for each follower voltage due to the sealed follower design. To obtain a spike form as shown in Fig. 3, V_{fna} rises with about 200 mV per ms, V_{fkd} rises with about 500 mV per ms.

Fig. 4 demonstrates spike trains for three different spiking modes. During fast spiking, only the basic spike mechanism is operating and interspike intervals (ISI) are of the same length (Fig. 4(a)). Regular spiking is with spike frequency adaptation (Fig. 4(b), AHP current on). The neuron initially fires at a high frequency and then adapts to a lower steady-state frequency: the rising V_c slowly increases the AHP current, which in turn progressively inhibits V_m. The parameters of the calcium circuit are tuned to have V_c dynamics as follows: calcium increase per spike is about 15 mV, calcium decay shows a time constant of about 100 ms. V_c increases between the first few spikes due to capacitive coupling across T1 (see Fig. 2). The AHP current has most influence between spikes in the subthreshold range of the neuron, where equation (1) is $I_{Cm} = I_{Leak} + I_{AHP} + I_{Inj}$. The AHP current must be stronger than the leakage current, otherwise it has hardly any effect on V_m.

Bursting is achieved by changing the potassium and AHP conductance when the neuron is in spike frequency mode (regular spiking). First, the maximal potassium conductance is significantly decreased, which leads to very fast spiking (not shown). Second, the AHP conductance is slightly decreased, which leads to bursting (Fig. 4(c)). During a burst the calcium level builds up and increases so the AHP current. After 3 to 5 spikes the AHP current is strong enough to interrupt the burst and to hyperpolarize V_m extensively due to the accumulated calcium level. The adaptive feedback loop runs until the calcium level is low again.

The input-output behavior of an adaptive neuron (for the regular spiking mode Fig. 4(b)) is analyzed by plotting instantaneous spike frequencies as a function of the step current amplitudes [5,13]. The instantaneous spike frequency is defined as the reciprocal of the ISI. Fig. 5(a) shows the frequency-current (F-I) curve for the parameters given for the spike train in Fig. 4(b). The first two step currents (1 and 2) are subthreshold stimulations. The following step currents (3 to 8) are suprathreshold stimulations. The instantaneous frequencies of the first eight ISIs are calculated. The first interval (f_1) shows a frequency range of 50 Hz (third stimulation current) to 190 Hz (8th stimulation current). The last three intervals (6 to 8) show a frequency range from 25 Hz to 60 Hz and we consider these as the steady-state frequency. The highest stimulus current is chosen to yield a f_1 of about 200 Hz. The AHPSAT is set high enough to yield a steady state frequency below 100 Hz. In Fig. 5(b), the instantaneous frequency is plotted as a function of time, to visualize the time course of adaptation. The decay in frequency is nonlinear and reaches steady state after about 50 ms.

To check the robustness of the neuron circuit, the remaining chips of the same series were tested with the same parameter values as in Fig. 5. Fig. 5(c) shows the F-I curves for another two chips. In Fig. 5(c), the frequencies are slightly smaller compared to the default F-I curve in Fig. 5(a). In Fig. 5(d), the frequencies are larger and adaptation occurs from

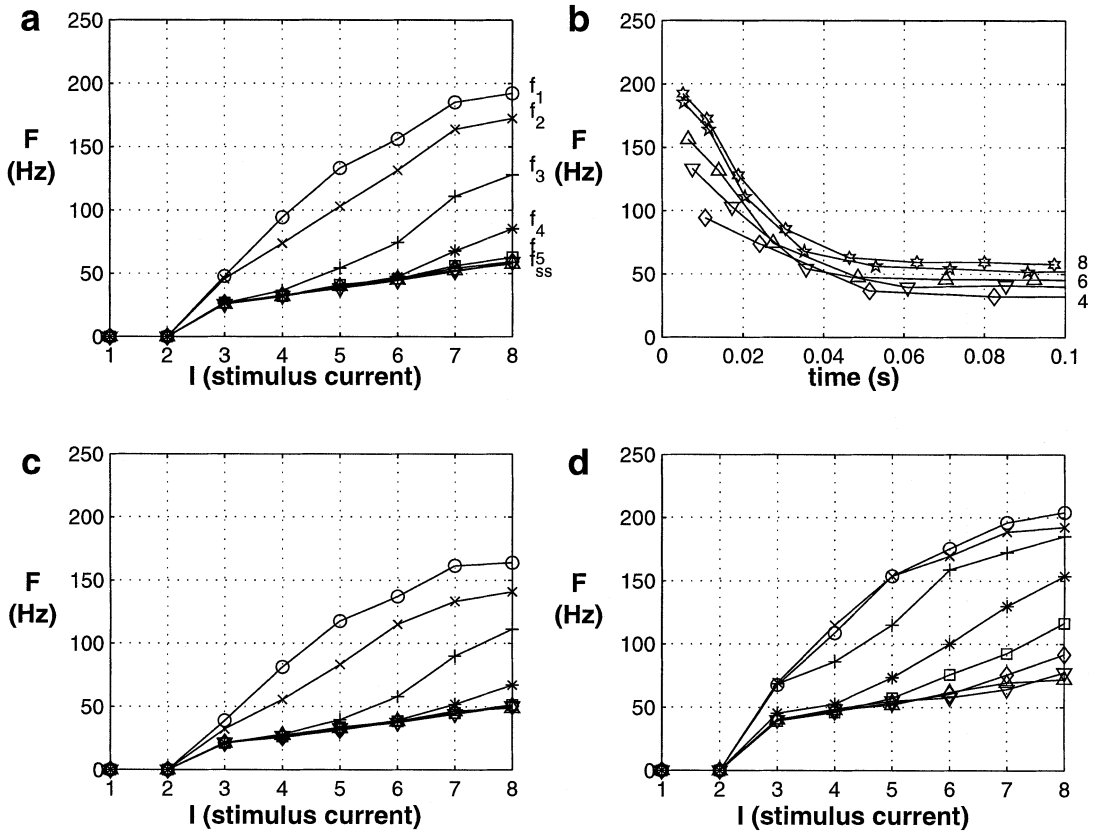

Fig. 5. Adaptation characteristics. (a) Frequency-current (F-I) curve. Step currents (1 to 8) ranging from approximately 20 nA to 340 nA of equal step are applied. The instantaneous spike-frequency (1/ISI) of the first 8 interspike intervals (ISI) are calculated. (b) Instantaneous frequency as a function of time, for the stimulus currents 4 to 8. Parameter values are the same as listed in the previous Fig. captions. (c) and (d) F-I curves from SNs from two different chips. Parameter values are identical to the ones for the F-I curve in (a).

the second interval on. Two of five chips of a series did not have proper spike-frequency adaptation. It seems that these chips contain severe mismatch due to the fabrication process.

4. Discussion

4.1. Improvements

The number of parameters required to control the basic spike mechanism has been reduced from 10 to 7 [10]. Three parameters were saved by reducing the threshold parameters from 3 to 1. In the sodium conductance, a single parameter (NASAT) instead of two is now used to control the maximal conductance. In previous neuron circuits, we could not simply connect the parameters because then the spike mechanism was not properly operating due to device mismatch. The reduction is now possible, because the followers are sealed such that the membrane spike is operated properly despite possible device mismatch.

In older adaptation circuits, the duration of the calcium influx depended on the width of the membrane spike, which made it extremely difficult to yield the appropriate FI curve. Therefore, the spike discriminator (not published previously) was extended by an edge-detecting circuit, that generates fixed width pulses independent of the membrane spike width. This allows us to tune the adaptation and bursting behavior in very short time.

In all previous circuits, an emulation of the calcium conductance was included. Because its effect on the spiking pattern was marginal and its tuning was

difficult, we omitted it in the present version. We simulate now the calcium influx by connecting the discriminator pulse directly onto the source of a p-type transistor emulating the calcium influx.

These modifications resulted in the following four new circuit features: First, the circuits are now robust. The present circuits allow us to change parameter values by tens of millivolts without losing the spiking pattern. All parameter values except the injection values were set to the second decimal place. Second, the number of parameters is reduced. Third, as a consequence of the first two features, the tuning of the parameter values can be performed within minutes. Fourth, bursting behavior is possible.

Differences in spike properties among chips are small Fig. 5(c). The parameter values are therefore sufficiently stable to be set by floating gate technology. This is a requirement if we use the SN for large-scale network simulations [1]. Except of the parameters EK and ENA, all parameter values are gate voltages, which can be easily stored on-chip. We have already succesfully applied the floating gate method to a previous neuron circuit [3]. The accuracy of setting the floating gates is about 3 mV, which is far less than the accuracy for setting the neurons parameters (about 10 mV). We therefore can expect that with the present neuron version initialization of the floating gates will be greatly facilitated because of the robustness and ease of setting the parameter values.

4.2. Tuning

In some paragraphs of the result section, we have given hints how to tune the neuron. We shortly summarize the tuning hints as an algorithm:

1. Passive behavior: The constant decay of V_m after offset of a step current should be about 500 mV/15 ms.
2. Spike behavior: Spike offset should occur at a low voltage, close to EK (Fig. 3). The AHP current has then a sufficient voltage range (THRES-EK = 1V) to inhibit V_m. The detailed spike dynamics do not play a crucial role. In our case we tuned the slopes of the follower voltages V_{fna} and V_{fkd} to values of 200 mV/ms and 500 mV/ms, respectively.
3. Calcium dynamics: The amplitude of calcium influx should be tuned to a fraction of the linear-range of the TCA (Fig. 4), in our case the amplitude is 15 mV. The decay time constant should be about 100 ms.
4. AHP conductance: The AHP conductance is increased until the steady state frequency is in a low-frequency range (Fig. 5) around 50 Hz.
5. Bursting: The maximal potassium conductance (KDSAT) is decreased by about 0.17 V. The AHP conductance (AHPSAT) is decreads by only a few millivolts (20 mV).

4.3. Correspondence to Real Neurons

In the Hodgkin-Huxley-formalism [4], an ion current has the following general form:

$$I_{Ion} = \overline{g}_{Ion} mh(V_m - E_{Ion}). \tag{13}$$

$\overline{g}_{Ion}$ is the maximal conductance of the ion current, m is an activation term, h is an inactivation term. Both terms can depend on time, voltage or substances, like for example calcium. The product mh represents the fraction of the maximal conductance. E_{Ion} is the reversal potential of the ion. The difference $(V_m - E_{Ion})$ is called the driving force (or electrotonic potential). The product mh plotted as a function of time, shows a typical shape for a particular ion current, which we will call now the activation function. In the silicon ion conductance circuits, the general dynamics of the activation functions are roughly approximated, rather than the details of the equation itself. TCAs generate currents which correspond to either an activation m or inactivation h. The parameter SAT (NASAT, KDSAT, AHPSAT) of the TCA is analogous to the maximal conductance $\overline{g}_{Ion}$. The voltage dependence of the TCA can be interpreted as being the voltage dependence of the term m or h. FI2 and FI3 determine the delay of the activation m or inactivation h and represent so the time dependence of the terms. The reversal potentials EK and ENA are analogous to the reversal potentials in real cells. They represent the battery for a particular ion current. A simulation of the driving force $(V_m - E_{Ion})$ is not incorporated in our circuits.

The sodium current circuitry dynamic resembles a typical fast sodium inward current, which typically is modeled by an activation function, m^3h [4,5]. The shape of this activation function is mimicked by a subtraction of an activation current and an inactiva-

tion current. The activation current lacks a delay element since it is supposed to turn on very quickly.

The real potassium outward current is only activating and therefore has only an activating term n, depending on voltage and time. The current turns on slowly and turns off when V_m is low again. The activation function in the HH formalism reads n^4, which shows a bell-shaped curve, plotted as a function of time. The silicon potassium circuit behaves similarly. The potassium current turns on at a rate given by FI3 and turns off when V_{fkd} is below THRES.

The parameters of the sodium and potassium conductance were tuned to generate spikes of plausible shape (Fig. 3). This leads to a spike width of about 0.6 ms, which is shorter than the spike width in real neurons (1-2 ms). The form of the spike would be altered if one choses larger spike widths. The shape of the spike above threshold looks then rather pulse-like: after V_m has hit ENA, it stays there for a short period, before the potassium conductance repolarizes V_m.

The real AHP current, a calcium-activated potassium current, has an activation function which is roughly linear to the calcium level. The silicon AHP current expresses the linearity m_{Ca} in the linear part of the tanh of the TCA.

The F-I curve in Fig. 5 is qualitatively the same as for real neurons (see [6] for a comparison). In real neurons the decay in (instantaneous) frequency is exponential and has finished after about 100–130 ms [13]. In the SN, the decay is nonlinear and adaptation has occured after about 50 to 60 ms Fig. 5(b). The lack of linear decay and long adaptation time constants is due to the non-ideal behavior of V_c.

4.4. Comparison and Use

Simoni and DeWeerth constructed a SN which has apparent similarities to our SN [12]. It also consists of a spiking and an adaptation mechanism. In contrast to our adaptive mechanism, their adaptation is adjusting the conductances of the spiking mechanism to make it robust to changes in a network. A similar adaptive mechanism was constructed by Shin and Koch to regulate our silicon neuron on a long-term scale [11]. It is not clear yet what the phenomenon of spike frequency adaptation is used for in a real cells [5]. But these issues can be addressed in a network simulation [1].

The improved neuron has already been used for other neuronal models, like dendritic models [8,10], where we show how the three different spiking modes affect a silicon dendritic cable.

Acknowledgments

We thank the following persons: Richard Hahnloser, Giacomo Indiveri, Jörg Kramer, Shih-Chii Liu for help on the manuscript; Philipp Häfliger, Dave Lawrence and Brian Baker for electronic support.

The work has been supported by the following institutions: the US Office of Naval Research (ONR) and Center Suisse d'Electronique et de Microtechnique (CSEM) and Schwerpunktprogramm (SPP) Biotechnologie des Schweizerischen Nationalfonds.

References

1. S. Deiss, R. J. Douglas, and A. Whatley, ''A pulse-coded communications infrastructure for neuromorphic systems.'' In *Pulsed Neural Networks*. chapter 6, pp. 157–178. The MIT Press, 1999.
2. Ph. Häfliger, *A spike based learning rule and its implementation in analog hardware*. Ph.D. thesis, Eidgenössische Technische Hochschule Zürich, Switzerland, 2000.
3. Ph. Häfliger and C. Rasche, ''Floating gate analog memory for parameter and variable storage in a learning silicon neuron.'' In *IEEE International Symposium on Circuits and Systems* 2, pp. 416–419, Orlando, 1999.
4. A. L. Hodgkin and A. F. Huxley, ''A quantitative description of membrane current and its application to conduction and excitation in nerve.'' *Journal of Physiology* 117, pp. 500–544, 1952.
5. C. Koch, *Biophysics of Computation: Information Processing in Single Neurons*. Oxford University Press, 1999.
6. M. Mahowald and R. Douglas, ''A silicon neuron.'' *Nature* 354, pp. 515–518, 1991.
7. C. A. Mead, *Analog VLSI and Neural Systems*. Addison-Wesley, Reading, Massachusetts, 1989.
8. C. Rasche, *Analog VLSI Circuits for Emulating Computational Features of Pyramidal Cells*. Ph.D. thesis, No. 13268, Eidgenössische Technische Hochschule Zürich, Switzerland, 1999.
9. C. Rasche, R. Douglas, and M. Mahowald, ''Characterization of a pyramidal silicon neuron.'' In *Neuromorphic Systems: Engineering Silicon from Neurobiology*. pp. 169–177. World Scientific, 1998.
10. C. Rasche and R. J. Douglas, *Forward- and backpropagation in a silicon dendrite*. 2000 (submitted).
11. J. Shin and C. Koch, ''Dynamic range and sensitivity adaptation in a silicon spiking neuron.'' *IEEE Trans. Neural Networks* 10(5), pp. 1232–1238, 1999.

12. M. F. Simoni and S. P. DeWeerth, ''Adaptation in an aVLSI model of a neuron.'' *IEEE Transactions on Circuits and Systems II: Analog and Digital Signal Processing* 46(7), pp. 967–970, 1999.
13. X. J. Wang, ''Calcium coding and adaptive temporal computation in cortical pyramidal neurons.'' *Journal of Neurophysiology* 79(3), pp. 1549–1566, 1998.
14. L. Watts, D. Kerns, R. Lyon, and C. Mead, ''Improved implementation of the silicon cochlea.'' *IEEE Journal of Solid-State Circuits* 27, pp. 692–700, 1992.

Christoph Rasche studied zoology at the University of Zürich. During his Ph.D. he built silicon neurons at the Institute of Neuroinformatics. He now works on a computer model of selective visual attention at the Klab at Caltech. See his homepage, http://klab.caltech.edu/~rasche, for details.

Rodney J. Douglas is co-director of the Institute of Neuroinformatics at the ETH/University of Zürich. His interests are neocortical microcircuits and their implementation into aVLSI. See his homepage, http://www.ini.unizh.ch/~rjd, for details.